Optical Fiber Technology 87 (2024) 103892

Contents lists available at ScienceDirect

Optical Fiber Technology

journal homepage: www.elsevier.com/locate/yofte

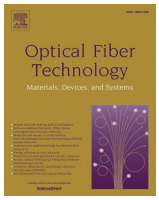

Regular Articles

Low noise operation of an all polarization-maintaining figure-9 Er:fiber laser with near-zero cavity dispersion

Haihao Cheng [a,b,1], Zhao Zhang [a,b,1], Xiaohong Hu [a,*], Ting Zhang [a,b], Ran Pan [a,b], Jing Jia [a,b], Yishan Wang [a,b], Shun Wu [a,c]

[a] State Key Laboratory of Transient Optics and Photonics, Xi'an Institute of Optics and Precision Mechanics, Chinese Academy of Sciences, Xi'an 710119, China
[b] University of Chinese Academy of Sciences, Chinese Academy of Sciences, Beijing 100049, China
[c] Hubei Key Laboratory of Optical Information and Pattern Recognition, Wuhan Institute of Technology, Wuhan 430205, China

ARTICLE INFO

Keywords:
All-PM figure-9 fiber laser
Relative intensity noise and timing jitter
Repetition rate locking

ABSTRACT

We demonstrate the low noise operation of a figure-9 1.5-μm Er:fiber laser constructed by all polarization-maintaining (PM) fiber and fiber components. Starting from the original rate equations and nonlinear Schrödinger equation, the cavity roundtrip evolution toward stable mode locking state is present. The radio frequency spectrum shows a 94.6-MHz fundamental repetition rate with up to 100 dB high signal-to-noise ratio. The net dispersion is tailored to near zero by incorporating and optimizing the length of PM dispersion-compensating fiber in the cavity. As a result, an integrated root-mean-square relative intensity noise of 0.0026 % [1 Hz, 1 MHz] and 10.8-fs timing jitter [100 Hz, 1 MHz] at the fundamental repetition rate are measured. We also lock the fundamental repetition frequency to a stable radio frequency reference and an in-loop relative stability of 2.1×10^{-12} at 1-s gate time is obtained.

1. Introduction

With the progress of fiber and fiber device fabrication technology, the optical performances of mode-locked femtosecond fiber lasers are improved greatly. The femtosecond lasers have played critical roles in many applications such as high precision machining [1,2], optical fiber frequency comb (OFC) [3,4], attosecond science [5,6], soliton dynamics research [7–9] and so on. Passively mode-locked fiber laser has the advantages of compactness, high stability and free-maintenance [10]. Unlike the real saturable absorber (SA), artificial SA will not encounter the problem of material properties degradation due to long-term use. Nonlinear polarization rotation or evolution (NPR, NPE) relies on the polarization effect of the fiber and thus are sensitive to the environmental perturbations. Although, it can be solved by rotating the splicing face of the polarization-maintaining (PM) fiber [11,12], the self-starting condition will be more severe, and one can not necessarily obtain the best mode-locking state due to the lack of polarization adjustability. Instead, the mode-locked all-PM fiber lasers based on nonlinear optical or amplifying loop mirror (NOLM, NALM) are good candidates for various outdoor applications, space microgravity environment [13,14] and vehicle environment [15].

In recent years, the figure-9 fiber lasers based on NALM were intensively studied. One seminal study in this area was the work of an all-PM fiber OFC based on NALM mode-locked Er:fiber laser reported by N. Kuse and the co-workers in 2016 [16]. In 2017, W. Hänsel et al demonstrated an innovative structure of the figure-9 fiber laser in which the nonreciprocal phase shifter (PS) was consisted of a Faraday rotator and a waveplate [17]. The splitting ratio could be fine optimized while keeping the maximum NALM transmission unchanged by slightly changing the angular direction of one PBS or inserting another half waveplate. As examples, at wavelength of 1565 nm, 250-MHz high repetition rate, 43-nm spectrum width were achieved based on this compact laser structure and close to zero cavity dispersion. In the same year, Feihong Chen et al. reported an NALM mode locked all-PM-fiber integrated Er:fiber laser. Femtosecond pulses with the repetition rates ranging from 48.8-64.7 MHz were realized [18]. In 2018, Guanyu Liu et al. reported a self-starting 700-MHz Yb:fiber laser which incorporated a phase biased non-PM NALM. The laser contained spatial optical components and can deliver an average power up to 150 mW. An integrated root-mean square (rms) relative intensity noise (RIN) of 0.015 %

* Corresponding author.
E-mail address: xhhu@opt.ac.cn (X. Hu).
[1] These authors contributed equally to this work.

https://doi.org/10.1016/j.yofte.2024.103892
Received 9 April 2024; Received in revised form 22 May 2024; Accepted 23 June 2024

([10 Hz, 10 MHz]) was obtained [19]. In 2019, Ke Yin et al. demonstrated a 121-MHz all-PM figure-9 fiber laser. The all-PM-fiber linear arm and the NALM ring were bridged through a 2 × 2 fiber coupler with a splitting ratio of 30:70 [20]. In 2022, Qinghui Deng et al. further boosted the repetition rate to 201.14 MHz by adopting a homemade highly integrated fiber component which contained a PS, a 50:50 splitter and a wavelength division multiplexer (WDM) [21]. In 2020, Yue Zhou et al. inserted a segment of PM dispersion-compensating fiber (DCF) in the cavity and tailored the net intracavity dispersion of a NALM Er:fiber laser to near zero. Experimentally, 41-MHz stretched pulses with a spectral width of 39.5 nm was achieved [22]. In 2021, Yihan Pi et al. demonstrated a 122-MHz, NALM based Er-doped fiber laser with a total net cavity dispersion of − 0.0107 ps^2. The integrated rms RIN of 0.004 % ([100 Hz, 1 MHz]) and rms timing jitter of 1.9 fs ([10 kHz, 1 MHz]) were realized. The linear arm part of the laser consisted of several spatial optical components including a half-wave plate, a polarization beam splitter and a piezoelectric ceramic transducer (PZT) mounted reflective mirror. A proportional-integral servo (Newfocus, LB1005) was further adopted to control this intracavity PZT and stabilize the repetition rate f_r to a fiber delay line [23]. In 2023, Haihao Cheng et al. quantified the noise properties of a figure-9 Er:fiber laser based on an all-PM fiber and fiber components integrated structure. The 103.4-MHz oscillator showed a net cavity dispersion of − 0.02 ps^2. The integrated rms RIN and timing jitter were 0.0056 % ([1 Hz, 1 MHz]) and 63.7 fs ([100 Hz, 1 MHz]), respectively [24]. Minghe Zhao et al further realized a 100-MHz, NALM mode locked Er: fiber laser on the “optical cube” structure. The net intracavity dispersion was − 0.0179 ps^2. The integrated rms timing jitter of 99.63 as ([10 kHz, 1 MHz]) and optimized rms RIN of 0.0399 % ([100 Hz, 100 kHz]) were obtained. In their laser, active stabilization of the f_r was achieved by mounting a PZT on the end mirror and the rms drift of f_r after locking was 10.72 mHz [25].

At the same time, the theoretical analyses combined with experimental investigations have been reported sporadically. In 2020, Aline S. Mayer et al. designed and fabricated a flexible ytterbium (Yb) fiber laser constructed by bulk components based linear arm and an all-PM fiber NALM [26]. They used the Jones matrix model to analyze the roundtrip transmission of the cavity under different splitting ratios. Five representative mode-locking states of different net cavity dispersion with the repetition rates all around 78 MHz were achieved. Very low integrated RIN of 0.003 % [1 Hz, 1 MHz] and rms timing jitter of 72 fs [100 Hz, 1 MHz] were obtained when the net intracavity dispersion was tailored close to zero.

In 2021, Yuxuan Ma et al. further reported an all-PM-fiber integrated 1.03 μm Yb:fiber laser mode-locked by NALM [27]. The authors theoretically analyzed the influences of the coupling ratio, YDF asymmetry, nonreciprocal phase shift and CFBG bandwidth on the mode locking performances. Finally, they obtained 54-MHz mode-locked pulses with an average output power of ~ 51 mW. The integrated RIN and rms timing jitter were measured as 0.0255 % [10 Hz, 1 MHz] and 0.7 fs [25 kHz, 5 MHz], respectively. In 2022, Shiping Xiong et al. presented theoretical analyses of NALM mode-locked Er:fiber lasers under asymmetric and weakly asymmetric conditions [28].

In this work, for a near-zero net cavity dispersion, we realized the low noise operation of a NALM mode-locked figure-9 Er:fiber laser constructed by all-PM fiber and PM-fiber components. Explicitly, 0.0026 % ([1 Hz, 1 MHz]) integrated rms RIN and 10.8-fs timing jitter ([100 Hz, 1 MHz]) at the fundamental repetition rate of 94.6 MHz were characterized. The integrated rms RIN is lower than the 0.004 % [100 Hz, 1 MHz] and 0.0399 % [100 Hz, 100 kHz] [23,25]. Meanwhile, the laser delivered stretched pulses with a center wavelength of 1563.7 nm, 2.2-mW average power and 3-dB spectral width of 48.7 nm. In addition, starting from the original time-independent rate equations and nonlinear Schrödinger equation, we also simulated the mode-locking processes corresponding to the near-zero intracavity dispersion case. The calculated optical spectrum accorded well with the measured one.

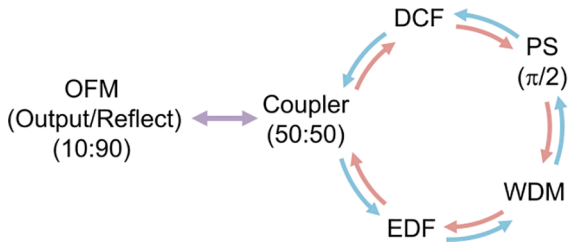

Fig. 1. Calculation flowchart of the all-PM figure-9 Er:fiber laser. OFM: optical fiber mirror, DCF: dispersion-compensating fiber, EDF: erbium-doped fiber, PS: phase shifter, WDM: wavelength division multiplexer, LD: laser diode.

2. Fiber laser principle and simulation

The schematic diagram of the proposed NALM mode-locked all-PM figure-9 Er:fiber laser is shown in Fig. 1. The linear arm and NALM loop bridged by a 50:50 fused PM fiber coupler jointly constitute the oscillator cavity. In the linear arm, the output/reflect ratio of the optical fiber mirror (OFM) is 10:90. The NALM loop is composed of ~ 36-cm long erbium-doped fiber (EDF), 19-cm long DCF, a π/2 PS, a WDM and the pigtails of fiber components. The PS in the NALM loop induces a π/2 nonreciprocal phase difference between the clockwise and counterclockwise propagated light. The pump light provided by a 976 nm laser diode (LD) is coupled into the NALM loop through a 980/1550 nm WDM.

In our works, DCF with positive group-velocity dispersion (GVD) play a crucial role in compensating the net cavity dispersion to near zero. The evolution processes of pulse along the fiber part are described by the well-known generalized nonlinear Schrödinger equation (GNLSE) [29]:

$$\frac{\partial A^{\pm}}{\partial z}+\frac{\alpha-g^{\pm}}{2}A^{\pm}+\frac{i\beta_2}{2}\frac{\partial^2 A^{\pm}}{\partial T^2}-\frac{\beta_3}{6}\frac{\partial^3 A^{\pm}}{\partial T^3} = i\gamma\left(|A^{\pm}|^2A^{\pm}+\frac{i}{\omega_0}\frac{\partial}{\partial T}\left(|A^{\pm}|^2A^{\pm}\right)-T_R A^{\pm}\frac{\partial|A^{\pm}|^2}{\partial T}\right) \quad (1)$$

Here, A is the complex electric field envelope, z is the propagation position, T is the time variable in delayed coordinate system, β_2 and β_3 represent the GVD and third-order dispersion (TOD) coefficients, g and α are the gain and loss coefficient, γ represents the Kerr nonlinear coefficient, ω_0 is the angular frequency corresponding to the central wavelength, T_R expresses the Raman response. The superscript ‘±’ represent the clockwise and anticlockwise direction, respectively. The right-hand side of the equation describes nonlinear terms including self-phase modulation (SPM), self-steepening and stimulated Raman scattering effects. Noting that the net intracavity dispersion is near to zero, it is necessary to consider the effects of TOD. According to [29], the pulse peak power does not reach the threshold of higher-order nonlinear effect, so the self-steepening and stimulated Raman scattering terms are not considered in the simulation process. To guide the following experiment, the repetition rate of the simulated laser is chosen to be 95 MHz.

After interfering in the fused fiber coupler, the complex amplitude of the transmitted and reflected field of the NALM loop can be obtained through Eq. (2).

$$\begin{bmatrix}A_T\\A_R\end{bmatrix}=\begin{bmatrix}\sqrt{\rho} & i\sqrt{1-\rho}\\ i\sqrt{1-\rho} & \sqrt{\rho}\end{bmatrix}\begin{bmatrix}A^{+}\exp\left(i\phi_0+i\phi_{NL}^{+}\right)\\A^{-}\exp\left(i\phi_0+i\phi_{NL}^{-}\right)\end{bmatrix} \quad (2)$$

Here, ρ is the splitting ratio of the fused fiber coupler. A^+ and A^- represent the complex amplitude of the clockwise- and anticlockwise-propagated fields, respectively. ϕ_0 is the linear phase shift accumulated in the NALM ring. ϕ_{NL}^{+} and ϕ^{-}_{NL} are the nonlinear phase shift induced by the self-phase and cross-phase modulation effects.

For our modeled Er:fiber laser, considering the fact that the EDF has

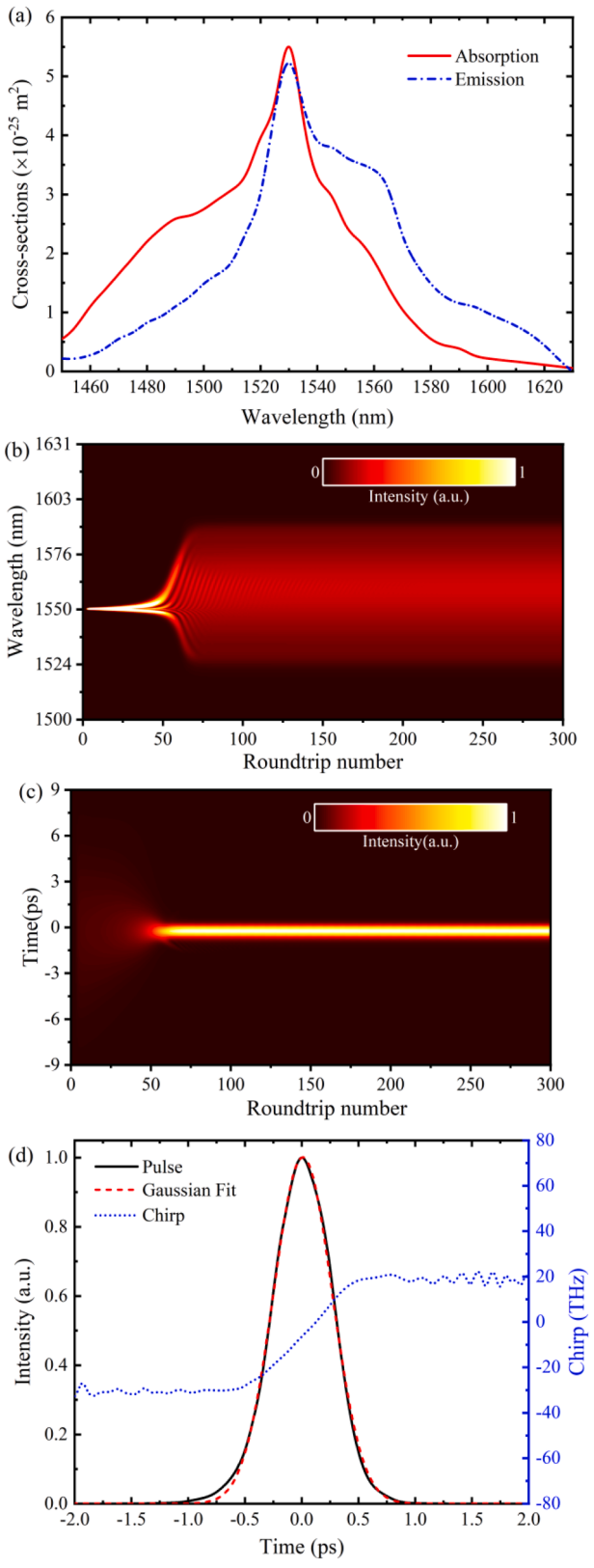

Fig. 2. (a) The absorption (red solid line) and emission (blue short dash-dotted line) cross sections, (b) The simulated spectrum and (c) pulse evolutionary diagrams with 300 cavity roundtrips. (d) The pulse intensity profile (black solid line), Gaussian fitting (red short dashed line) and the chirp (blue short dashed line) profile at the 300th roundtrip. (For interpretation of the references to colour in this figure legend, the reader is referred to the web version of this article.)

Table 1
Parameters used in our simulation.

Item	Symbol	Value
Physical constant		
Velocity of light	c	2.99792458×10^{8} m/s
Planck's constant	h	$6.62607015 \times 10^{-34}$ J·s
PM-EDF		
Population of Er^{3+} ions	N	5.92×10^{25} (ions/m^3)
Mode field area	EDF-A_{eff}	26.42 μm^2
Signal wavelength	λ_s	1550 nm
Pump wavelength	λ_p	976 nm
Signal power filling factor [33]	Γ_s	0.694
Pump power filling factor [33]	Γ_p	0.889
Pump emission cross section [33]	σ_{ep}	2×10^{-27} m^2
Pump absorption cross section [33]	σ_{ap}	2×10^{-25} m^2
Spontaneous radiation lifetime	τ	10 ms
Group-velocity dispersion	EDF-β_2	0.02804 ps^2/m
Third-order dispersion	EDF-β_3	-6.876×10^{-5} ps^3/m
Kerr nonlinear coefficient	EDF-γ	3.8 W^{-1}·km^{-1}
PM-DCF		
Mode field area	DCF-A_{eff}	20 μm^2
Group-velocity dispersion	DCF-β_2	0.1275 ps^2/m
Third-order dispersion	DCF-β_3	-7.56×10^{-4} ps^3/m
Kerr nonlinear coefficient	DCF-γ	4.5 W^{-1}·km^{-1}
PM-SMF		
Mode field area	SMF-A_{eff}	86.59 μm^2
Group-velocity dispersion	SMF-β_2	−0.02167 ps^2/m
Third-order dispersion	SMF-β_3	1.907×10^{-4} ps^3/m
Kerr nonlinear coefficient	SMF-γ	1.0 W^{-1}·km^{-1}
Insertion losses of the fiber components		
Phase shifter		0.37 dB
Wavelength division multiplexer		0.56 dB
Optical fiber mirror		1.18 dB (Input-Input)
		11.8 dB (Input-Output)
Fusion losses		
PM-EDF to PM-SMF		0.5 dB
PM-DCF to PM-SMF		1.0 dB

a single cladding and a highly doped core, hence, instead of the gain saturation model [28], we calculate the variation of the gain coefficient g along the EDF starting from the original steady-state rate (3)-(5) [30,31] of a simplified two-level laser system. The scattering loss and amplified spontaneous emission are ignored in the calculation process.

$$\frac{N_2(z)}{N} = \frac{\frac{P_p(z)\sigma_{ap}\Gamma_p}{h\nu_p A_{core}} + \frac{\Gamma_s}{hcA_{core}}\int \sigma_{as}(\lambda)P_s(z,\lambda)\lambda d\lambda}{\frac{P_p(z)(\sigma_{ap}+\sigma_{ep})\Gamma_p}{h\nu_p A_{core}} + \frac{1}{\tau} + \frac{\Gamma_s}{hcA_{core}}\int [\sigma_{as}(\lambda)+\sigma_{es}(\lambda)]P_s(z,\lambda)\lambda d\lambda} \tag{3}$$

$$\frac{dP_p(z)}{dz} = -\Gamma_p\left[\sigma_{ap}N - (\sigma_{ap}+\sigma_{ep})N_2(z)\right]P_p(z) \tag{4}$$

$$\frac{dP_s(z,\lambda)}{dz} = \Gamma_s\{[\sigma_{as}(\lambda)+\sigma_{es}(\lambda)]N_2(z) - \sigma_{as}(\lambda)N\}P_s(z,\lambda) \tag{5}$$

where g of Eq. (1) is the power gain coefficient at different position z of EDF and can be obtained through Eq. (5) [30]. P_s, P_p are the average power of the signal and pump laser, respectively. N represents the total population of Er^{3+} ions. The pump power filling factor Γ_p reflects the fraction of pump power which is actually coupled into the Er^{3+} doped fiber core and can be estimated by the ratio between the area of the geometrical core and the mode field area. Γ_s is signal power filling factor of the lowest order LP_{01} mode in the core. λ_p, λ_s denote the pump and signal wavelengths, respectively. σ_{ap}, σ_{as} are the pump and signal absorbing cross section. σ_{es} and σ_{ep} expresses the emission cross section at the signal and pump wavelength. The parameters ν_s, A_{core} and τ represent the signal frequency, cross-sectional area of the fiber core, and the upper-level lifetime. h and c are the Planck's constant and the speed of light in vacuum, respectively. It should be noted that the gain

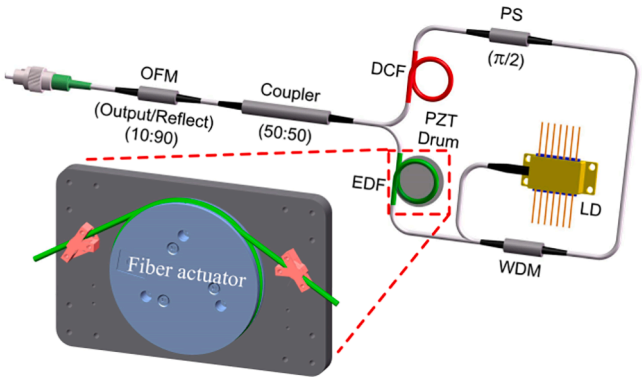

Fig. 3. Schematic diagram of the repetition-rate locked, all-PM figure-9 Er:fiber laser with a near-zero cavity dispersion. OFM: optical fiber mirror, DCF: dispersion-compensating fiber, EDF: erbium-doped fiber with a peak core absorption of 72 dB/m at 1530 nm, PZT Drum: piezoelectric transducer driven, drum like mechanical gear, PS: phase shifter, WDM: wavelength division multiplexer, LD: laser diode.

saturation model was established based on the assumption of $N_2 \ll N$, in which N_2 is the upper lasing level population density [30,31]. In Fig. 1, noting that for the amplification process of the counter-clockwise propagated pulse, the initial pump power is unknown. In the simulation process, it is determined by using the trial-and-error method until the pump power is self-consistent and a stable mode locking state is achieved [30]. The Eqs. (4) and (5) gives the variation of the pump and signal power along the propagation distance. The GNLSE are numerically solved by using the symmetric distribution Fourier method with an initial input pulse of weak energy and wide duration. The evolution starting and end points are both the output fiber mirror in the linear arm. The calculation procedure is displayed in Fig. 1. Fig. 2 depicts the evolution of the pulse and spectrum with up to 300 total cavity roundtrips. In addition, we find that the self-starting of a stable mode-locked state is easier when the DCF is located between the 50:50 fused fiber coupler and the PS.

Table 1 summarizes all the parameters used in the simulation. The total population density N of the EDF is calculated according to the measured peak core absorption at 1530-nm wavelength. The wavelength dependent emission and absorption cross sections of the EDF used in the simulation can be found in Ref. [32], as shown in Fig. 2(a).

We choose the $\pi/2$ PS for the phase bias both in the numerical simulation and experimental realization of the laser for a comprehensive consideration between the output power and the spectral bandwidth [27,28]. In addition, a 50:50 coupler is selected in the calculation and experiment. The DCF length is determined so that a near-zero net cavity dispersion is arrived.

In the simulation, we found that the location of DCF can greatly affect the self-starting threshold, temporal pulse and spectrum evolution processes etc. For example, when the DCF is placed either before or after the EDF, the pulse propagated in the counter-clockwise direction will undergo a large broadening process due to the high positive GVD of the DCF. Obviously, this will greatly reduce the peak power and thus the nonlinear phase difference between the bidirectionally propagated pulses. As a result, the fiber laser cannot operate in stable mode-locking states when the other cavity parameters are kept the same. Meanwhile, considering the high splicing loss (~1.0 dB) of the DCF, the 976-nm pump light injected from the WDM will experience a large loss, which is not advantageous for the establishment and self-starting of stable mode locking states.

3. Fabrication of figure-9 fiber laser and repetition frequency stabilization

The all-PM figure-9 fiber laser is illustrated in Fig. 3. The linear arm includes an optical fiber mirror (AFR-PMOFMI, 90:10) which is a coupler with a nominal output ratio of 10 % and an isolator hybrid component. The pigtailed fiber is ~ 12-cm long standard Panda-type SMF. In the NALM loop, the gain fiber is ~ 36-cm long PM-EDF (nLIGHT, Er80-4/125-HD-PM, peak core absorption of 72 dB/m @1530 nm). The pump light provided by a 976-nm LD is coupled into the NALM loop through a reflection-type 980/1550 nm WDM. The PS induces an $\pi/2$ phase difference between the clockwise and counter-clockwise propagated light. The PM-DCF (OFS, PMDCF) with a large positive GVD is used to compensate and optimize the net cavity dispersion to near zero. Noting that all the fiber and fiber components used to build the oscillator are PM type. The GVD parameters of SMF, EDF and DCF are approximately − 0.02167 ps^2/m, 0.02084 ps^2/m and 0.1275 ps^2/m at 1550-nm wavelength, respectively. For ~ 95-MHz repetition rate and close to zero net cavity dispersion, the length of PM-DCF is finally optimized to around 19 cm.

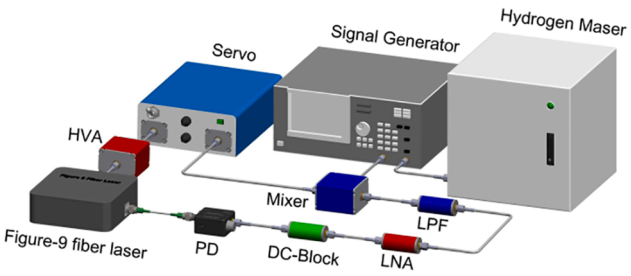

Fig. 4. Pilot circuit of the phase locked loop for the repetition frequency locking. HVA: high voltage amplifier, PD: photo-detector, LNA: low noise amplifier, LPF: low pass filter.

A commercial fusion splicer (Fujikura 100P +) was utilized to fabricate our all-PM figure-9 Er:fiber laser. Compared with PM-SMF, the PM-DCF exhibits smaller mode field diameters (MFD) and ring of highly fluorine doped trench [24,34]. After carefully optimizing the fusion parameters, we obtained ~ 1 dB splicing loss between the PM-DCF and PM-SMF. For the splicing between PM-EDF and PM-SMF, the standard PM-SMF splicing procedure was adopted.

Technically, by tracing the f_r of the oscillator to an atomic clock, one can greatly increase the f_r stability. f_r stabilization can further boost the application performances of femtosecond fiber lasers, such as the generation of high-stability optical frequency standard [35], the accuracy improvement in absolute distance measurement and laser ranging [36]. The repetition frequency actuator we used was based on a piezoelectric (PZT) driven, drum like mechanical gear and around 30-cm long EDF in the oscillator was wound on the actuator.

The phase locked loop (PLL) pilot circuit adopted to stabilize the repetition frequency is displayed in Fig. 4. The output pulses with an average power of 2.2 mW were detected through a 3-GHz InGaAs PD (Thorlabs, DET08CFC). Then, the RF signal was amplified by a low noise amplifier (LNA) and the fundamental repetition rate was filtered out through a low pass filter (LPF). The pure fundamental repetition rate was mixed with the reference signal delivered from an analog signal generator (Agilent Technologies, E8257D) which was simultaneously calibrated by a hydrogen maser (iMaser 3000). The error signal output from the mixer was then delivered into a servo controller (New Focus, LB1005). After 20 × amplification, the high voltage control signal was directly adopted to drive the PZT installed in the fiber actuator. Eventually, the repetition rate was locked and the frequency stability could be optimized by carefully tuning the servo control parameters.

4. Results and analysis

Considering that both the positive and negative dispersion fibers were used in the cavity, the net intracavity dispersion was estimated to

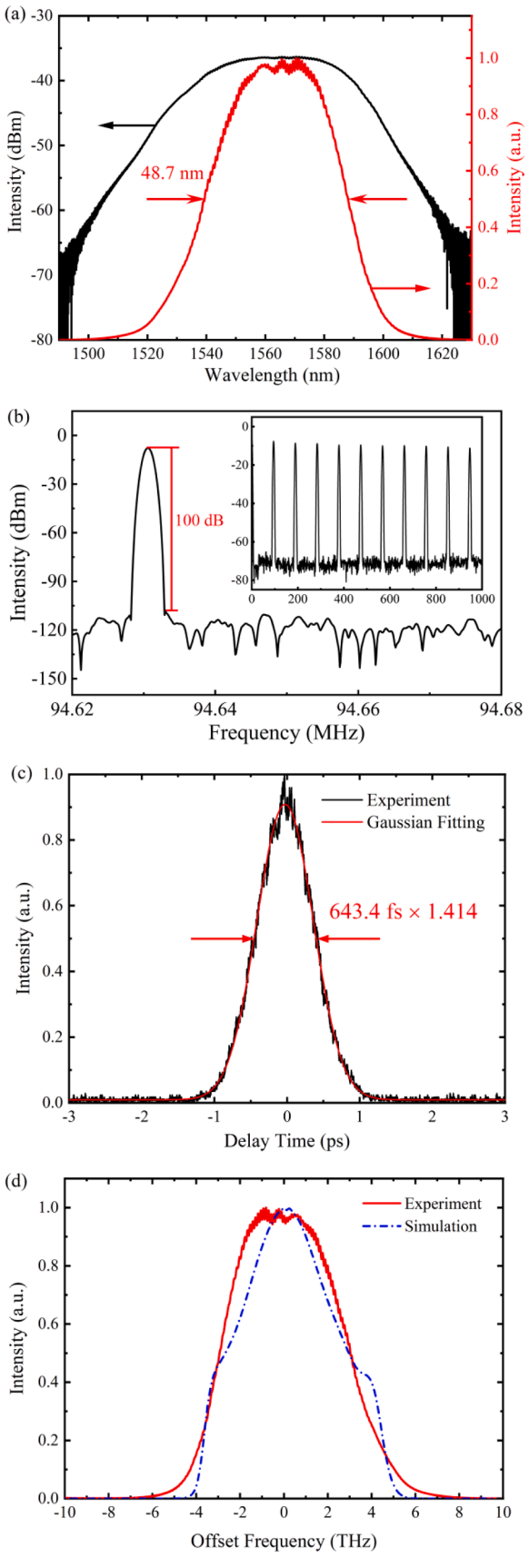

(caption on next column)

Fig. 5. (a) The measured optical spectra in the linear (red solid line) and logarithmic (black solid line) coordinates. (The 3-dB spectral bandwidth is indicated by two red arrows) (b) Radio-frequency (RF) spectrum of the all-PM figure-9 Er:fiber laser. Inset: broadband RF spectrum with a frequency span of 1000 MHz. The resolution bandwidth (RBW) and video bandwidth (VBW) of the phase noise analyzer were simultaneously set as 1 kHz and 3 MHz (inset), respectively. (c) Pulse autocorrelation trace. (d) Comparison between the simulated (blue short dash-dotted line) and experimental (red solid line) measured spectra. (For interpretation of the references to colour in this figure legend, the reader is referred to the web version of this article.)

be ~ -0.0002 ps^2. For a pump current of 320 mA, as displayed in Fig. 5 (a), the central wavelength located at 1563.7 nm and the FWHM spectral width of 48.7 nm was measured. Meanwhile, the laser delivered an average output power of 2.2 mW (Thorlabs, PM100D power meter). The RF spectrum of the 94.6-MHz fundamental repetition rate measured by an InGaAs PD (Thorlabs, DET08CFC) with 3-GHz bandwidth and a phase noise analyzer (Rohde & Schwarz, FSWP50) was shown in Fig. 5 (b). The signal to noise ratio (SNR) was up to ~ 100 dB. The inset of Fig. 5 (b) displayed the harmonic RF spectra at a resolution bandwidth (RBW) of 3 MHz and a frequency span of 1000 MHz. There was no sinusoidal modulation or other frequency components, which indicated that a stable single-pulse mode-locked state was achieved. The pulse autocorrelation trace displayed in Fig. 5 (c) was measured by a commercial autocorrelator (Femtochrome, FR103MN). A pulse duration of 643.4 fs was indicated by assuming a Gaussian profile. Fig. 5 (d) showed the comparison of the experimentally measured and numerically calculated optical spectra. The simulated spectrum was slightly narrower than the measured one both in the center and two wings, but the widths of the two spectra were almost the same. This may originate from the fact that the adopted absorption and emission curves of the EDF were slightly different from the actual ones.

In order to evaluate the noise performance of the figure-9 Er:fiber laser operating with a close to zero net cavity dispersion, we measured both the amplitude noise (AN) and phase noise (PN) at the fundamental repetition rate, as shown in Fig. 6. First, we used a PD (Thorlabs, DET08CFC, 5-GHz bandwidth, no amplifier) powered by a 12 V dry battery to convert the optical pulses into an electrical signal. The phase noise analyzer (Rohde & Schwarz, FSWP50) was then used to measure the single-sideband power spectral density (PSD) spectra. For AN or RIN measurement, the AM mode of the phase noise analyzer with a correlation factor of 100 was used. At a pump current of 320 mA, the measured single-sideband PSD spectrum of AN is present in Fig. 6 (a). For an offset frequency range from 1 Hz to 1 MHz, the rms RIN is 0.0026 %. The RIN-PSD values corresponding to the offset frequencies of 10 kHz and 100 kHz are −150 dBc/Hz and −156 dBc/Hz, respectively. It can be clearly seen that an overshoot occurs at an offset frequency of ~ 5 kHz which is the characteristic of the relaxation oscillation originating from the finite upper-state lifetime.

The technology noise induced by the driving circuit of the pump laser diode results in the noise peak at an offset frequency of around 25 kHz [24]. The noise floor determined by the vacuum fluctuation or shot noise which originates from the output coupler (OFM) of the oscillator can be calculated [37]. For 2.2-mW output power corresponding to a pump current of 320 mA, the shot noise limited RIN-PSD floor is about − 159 dBc/Hz. In addition, the PD shot noise determined RIN-PSD floor calculated is − 158 dBc/Hz. The RIN measurement above 40-kHz Fourier frequency is mainly limited by the PD shot noise.

We also obtained the PN PSD spectrum at the fundamental repetition rate in the experiment. The corresponding timing jitter PSD spectrum with an offset frequency span from 100 Hz to 1 MHz and a correlation factor of 100 is shown in Fig. 6 (b). The integrated timing jitter is 10.8 fs. For an offset frequency range from 100 Hz to 1 kHz, the timing jitter PSD decreases by 20 dB and it drops 10 dB from 1 kHz to 100 kHz.

The fiber laser mode locked by NALM has an inherent amplitude noise-suppression mechanism due to the interaction of the sinusoidal

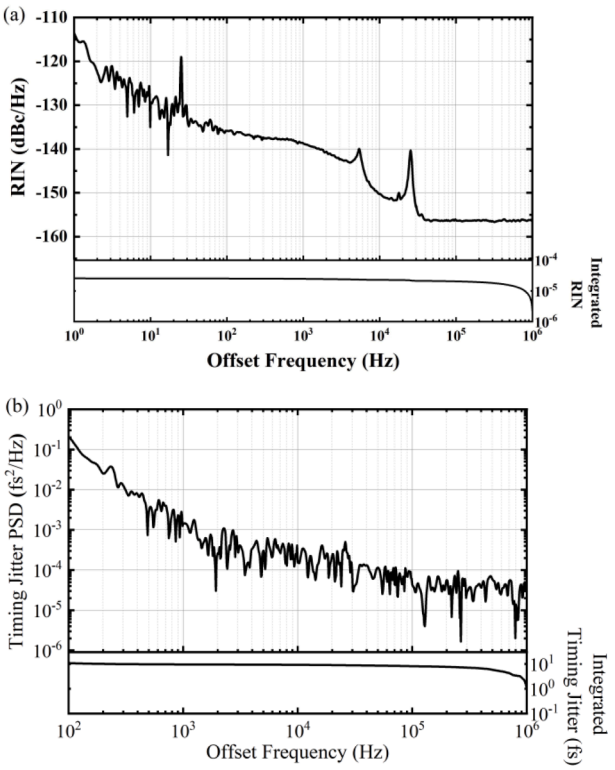

Fig. 6. Single-sideband noise power spectral density (PSD) spectra and integrated RMS (a) RIN and (b) timing jitter at the fundamental repetition frequency. The pump current is 320 mA.

transmission function with the fluctuating intracavity pulse amplitude [38]. Because the RIN reflects the fluctuation of the average power in essential, for pulsed laser, this also corresponds to a fluctuation of the intracavity pulse peak power. In this case, the nonlinear phase difference between the clockwise and anticlockwise propagated pulses can be expressed by Eq (6):

$$\overline{\Delta\varphi_{nl}} + \delta\Delta\varphi_{nl}(t) = \frac{\pi}{\lambda_s A_{eff}} n_2 g(\bar{P} + \delta P[t])(L_{CCW}\varepsilon - L_{CW}[1-\varepsilon]) \quad (6)$$

where the parameter $\delta P[t]$ denotes the fluctuation of the pulse peak power, λ_s, A_{eff}, n_2 represent the center wavelength of the pulse, the fiber effective mode area and nonlinear refractive index, respectively. g is the power gain factor and can be assumed the same for the counter-propagating pulses when an optical splitter with an energy splitting ratio of ε=0.5 is adopted. L_{ccw} and L_{cw} are the effective nonlinear optical paths. As is well known that the transmission of NALM is a function of the nonlinear phase shift and thus the function of the fluctuated intracavity pulse peak power. As a result, the transmission of NALM can be interpreted as a noise transfer function for the intracavity pulse amplitude fluctuations to the output ports. The studies of Ref. [38] further show that the resulting noise transfer enables a suppression of the accumulated AM-noise during each roundtrip due to an inversely proportional response of the NALM transmission to the intracavity pulse peak power fluctuations for a negative derivative of transmittance.

On the other hand, for the phase noise suppression, the main measure we have taken is tailoring the net cavity dispersion to near zero (e. g. -0.0002 ps^2) by inserting $\sim$ 19 cm long dispersion-compensating fiber in the NALM loop. As is pointed out in Ref. [37], this can greatly reduce the Gordon-Haus noise which in essence represents the amplified spontaneous emission (ASE) noise induced pulse center frequency fluctuation. This frequency fluctuation can be indirectly converted to timing jitter through dispersion. Meanwhile, the low RIN property of the fiber laser is also helpful for the reach of low timing jitter because the intensity noise coupled timing jitter (e. g. through Kramers-Kronig phase change in the gain medium and self-steepening effect) are greatly reduced.

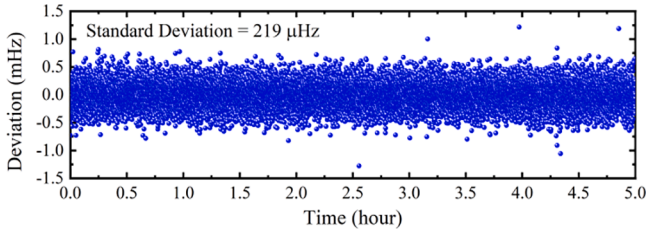

Fig. 7. The fluctuation of f_r after locking with a total lasting time of 5 h. The gate time is set as 1 s.

The fundamental repetition rate of our oscillator was further increased to $\sim$ 103.7 MHz. The PPL mentioned in section 3 was used to lock f_r. After locking, the f_r was monitored and recorded by using a frequency counter (Keysight, 53230A) with a gate time of 1 s. The standard deviation of 219 μHz was estimated based on the f_r data with a total lasting time of 5 h, as displayed in Fig. 7. The in-loop relative frequency stability was 2.1×10^{-12} (1-s gate time).

5. Conclusion

In brief, low noise operation of a figure-9 Er:fiber laser with near-zero cavity dispersion is demonstrated. The feasibility of stable mode locking is verified by solving the steady-state rate equations and nonlinear Schrödinger equation. The figure-9 fiber laser operating at 1563.7 nm delivers 94.6-MHz femtosecond pulse train. The RF spectrum of the fundamental repetition rate exhibits a 100 dB high SNR. In addition, an integrated rms timing jitter of 10.8 fs ([100 Hz, 1 MHz]) is measured. The low noise operation of the laser mainly benefits from the near-zero cavity dispersion and small cavity output ratio. The repetition frequency of the laser is increased to 103.7 MHz and after locking, the repetition frequency exhibits a relative stability of 2.1×10^{-12} at 1-s gate time. We proved the availability of 100-MHz-level, near-zero net intracavity dispersion, low noise figure-9 Er:fiber laser based on all-PM fiber and PM-fiber components integrated structure. The reported figure-9 Er:fiber laser has many applications, such as spectroscopy, precision distance measurement, low noise fiber optical frequency combs, etc.

Funding

Western Young Scholars Program of CAS (XAB2020YN11), Natural Science Foundation of China (NSFC) (61875227) and the Open Research Fund of State Key Laboratory of Transient Optics and Photonics (SKLST202105).

CRediT authorship contribution statement

Haihao Cheng: Writing – original draft, Methodology, Formal analysis, Conceptualization. **Zhao Zhang:** Validation, Investigation. **Xiaohong Hu:** Writing – review & editing, Writing – original draft, Project administration, Formal analysis, Data curation. **Ting Zhang:** Validation, Investigation. **Ran Pan:** Validation, Resources. **Jing Jia:** Validation, Resources. **Yishan Wang:** Supervision, Project administration, Funding acquisition. **Shun Wu:** Validation, Funding acquisition.

Declaration of competing interest

The authors declare that they have no known competing financial interests or personal relationships that could have appeared to influence the work reported in this paper.

Data availability

Data will be made available on request.

References

[1] Z.Y. Lin, M.H. Hong, Femtosecond laser precision engineering: from micron, submicron, to nanoscale, Ultrafast Science 3 (2021) 9783514, https://doi.org/10.34133/2021/9783514.

[2] J.L. Yong, Q. Yang, X. Hou, F. Chen, Nature-inspired superwettability achieved by femtosecond lasers, Ultrafast Science 4 (2021) 9895418, https://doi.org/10.34133/2022/9895418.

[3] Y.J. Cai, T. Zhang, R. Pan, X.H. Hu, F. Ye, W. Zhang, W. Zhao, Y.S. Wang, Compact, high-performance all-polarization-maintaining Er:fiber frequency comb with single fiber actuator, IEEE Photonics J. 12 (2020) 7102508, https://doi.org/10.1109/JPHOT.2020.3010558.

[4] Y.J. Cai, R. Pan, X.H. Hu, Y. Feng, W. Zhang, W. Zhao, Y.S. Wang, Phase-locked two-color visible frequency comb system based on 1.5-μm all-polarization-maintaining fiber laser, Opt. Eng. 59 (2020) 026107, https://doi.org/10.1117/1.OE.59.2.026107.

[5] P. Ye, L.G. Oldal, T. Csizmadia, Z. Filus, T. Grósz, P. Jójárt, I. Seres, Z. Bengery, B. Gilicze, S. Kahaly, K. Varjú, B. Major, High-flux 100 kHz attosecond pulse source driven by a high-average power annular laser beam, Ultrafast Science 1 (2022) 9823783, https://doi.org/10.34133/2022/9823783.

[6] T. Matsubara, Y. Nabekawa, K.L. Ishikawa, K. Yamanouchi, K. Midorikawa, Attosecond optical and ramsey-type interferometry by postgeneration splitting of harmonic pulse, Ultrafast Science 3 (2022) 9858739, https://doi.org/10.34133/2022/9858739.

[7] D. Mao, H.Q. Wang, H.Z. Zhang, C. Zeng, Y.Q. Du, Z.W. He, Z.P. Sun, J.L. Zhao, Synchronized multi-wavelength soliton fiber laser via intracavity group delay modulation, Nat. Commun. (2021) 6712, https://doi.org/10.1038/s41467-021-26872-x.

[8] D. Mao, Z.W. He, Y.S. Zhang, Y.Q. Du, C. Zeng, L. Yun, Z.C. Luo, T.J. Li, Z.P. Sun, J. L. Zhao, Phase-matching-induced near-chirp-free solitons in normal-dispersion fiber lasers, Light-Sci. Appl. 11 (2022) 25, https://doi.org/10.1038/s41377-022-00713-y.

[9] H.Z. Zhang, Y.Q. Du, C. Zeng, Z.P. Sun, Y. Zhang, J.L. Zhao, D. Mao, The dissipative Talbot soliton fiber laser, Sci. Adv. (2024) eadl2125, https://doi.org/10.1126/sciadv.adl2125.

[10] Y. Han, Y.B. Guo, B. Gao, C.Y. Ma, R.H. Zhang, H. Zhang, Generation, optimization, and application of ultrashort femtosecond pulse in mode-locked fiber lasers, Prog. in Quant. Electron. 71 (2020) 100264, https://doi.org/10.1016/j.pquantelec.2020.100264.

[11] W.C. Zhang, Y. Liu, C. Wang, Z.W. Zhu, D.P. Luo, C.L. Gu, W.X. Li, Ultrafast PM fiber ring laser mode-locked by nonlinear polarization evolution with short NPE section segments, Opt. Express 26 (2018) 7934–7941, https://doi.org/10.1364/OE.26.007934.

[12] L. Zhou, Y. Liu, G.H. Xie, W.C. Zhang, Z.W. Zhu, C. Ouyang, C.L. Gu, W.X. Li, Generation of stretched pulses from an all-polarization-maintaining Er-doped mode-locked fiber laser using nonlinear polarization evolution, Appl. Phys. Express 12 (2019) 052017, https://doi.org/10.7567/1882-0786/ab15c0.

[13] M. Lezius, T. Wilken, C. Deutsch, M. Giunta, O. Mandel, A. Thaller, V. Schkolnik, M. Schiemangk, A. Dinkelaker, A. Kohfeldt, A. Wicht, M. Krutzik, A. Peters, O. Hellmig, H. Duncker, K. Sengstock, P. Windpassinger, K. Lampmann, T. Hülsing, T.W. Hänsch, R. Holzwarth, Space-borne frequency comb metrology, Optica 3 (2016) 1381–1387, https://doi.org/10.1364/OPTICA.3.001381.

[14] B.J. Pröbster, M. Lezius, O. Mandel, C. Braxmaier, R. Holzwarth, FOKUS II—Space flight of a compact and vacuum compatible dual frequency comb system, J. Opt. Soc. Am. B 38 (2021) 932–939, https://doi.org/10.1364/JOSAB.413929.

[15] L.C. Sinclair, I. Coddington, W.C. Swann, G.B. Rieker, A. Hati, K. Iwakuni, N. R. Newbury, Operation of an optically coherent frequency comb outside the metrology lab, Opt. Express 22 (2014) 6996–7006, https://doi.org/10.1364/OE.22.006996.

[16] N. Kuse, J. Jiang, C.C. Lee, T.R. Schibli, M.E. Fermann, All polarization-maintaining Er fiber-based optical frequency combs with nonlinear amplifying loop mirror, Opt. Express 24 (2016) 3095–3102, https://doi.org/10.1364/OE.24.003095.

[17] W. Hänsel, H. Hoogland, M. Giunta, S. Schmid, T. Steinmetz, R. Doubek, P. Mayer, S. Dobner, C. Cleff, M. Fischer, R. Holzwarth, All polarization-maintaining fiber laser architecture for robust femtosecond pulse generation, Appl. Phys. B 123 (2017) 1–6, https://doi.org/10.1007/s00340-016-6598-2.

[18] F.H. Chen, Q. Hao, H.P. Zeng, Optimization of an NALM mode-locked all-pM Er: fiber laser system, IEEE Photonic Tech. l. 29 (2017) 2119–2122, https://doi.org/10.1109/LPT.2017.2765686.

[19] G.Y. Liu, X.H. Jiang, A.M. Wang, G.Q. Chang, F. Kaertner, Z.G. Zhang, Robust 700 MHz mode-locked Yb:fiber laser with a biased nonlinear amplifying loop mirror, Opt. Express 26 (2018) 26003–26008, https://doi.org/10.1364/OE.26.026003.

[20] K. Yin, Y.M. Li, Y.B. Wang, X. Zheng, T. Jiang, Self-starting all-fiber PM Er:laser mode locked by a biased nonlinear amplifying loop mirror, Chin. Phys. B 28 (2019) 124203, https://doi.org/10.1088/1674-1056/ab4d42.

[21] Q.H. Deng, K. Yin, J.H. Zhang, X. Zheng, T. Jiang, A 200 MHz compact environmentally-stable mode-locked Figure-9 fiber laser, IEEE Photon. J. 13 (2021) 1500605, https://doi.org/10.1109/JPHOT.2021.3095159.

[22] Y. Zhou, Y.W. Zeng, J. Yin, T. Dong, L.J. Sun, Y. Zhang, K. Xu, All-polarization-maintaining figure-of-9 soliton and dispersion-managed Er-doped fiber oscillators, Laser Phys. 30 (2020) 045101, https://doi.org/10.1088/1555-6611/ab7a99.

[23] Y.H. Pi, H.C. Tian, R.M. Li, Y. Han, Y.J. Song, M.L. Hu, Timing jitter and intensity noise characterization of a 122-MHz All-PM NALM mode-locked fiber laser, IEEE Photonics Tech. l. 33 (2021) 1439–1442, https://doi.org/10.1109/LPT.2021.3125994.

[24] H.H. Cheng, Z. Zhang, R. Pan, T. Zhang, Y. Feng, X.H. Hu, Y.S. Wang, S. Wu, Compact, repetition rate locked all-PM fiber femtosecond laser system based on low noise fgure-9 Er:fiber laser, Opt. Laser Technol. 158 (2023) 108818, https://doi.org/10.1016/j.optlastec.2022.108818.

[25] M.H. Zhao, R.A. Yang, X.G. Jin, Z.Y. Chen, A.M. Wang, Z.G. Zhang, Q. Li, Attosecond timing jitter from an NALM mode-locked Er:fiber laser on "optical cubes", J. Lightwave Technol. 42 (2023) 1651–1658, https://doi.org/10.1109/JLT.2023.3326068.

[26] A.S. Mayer, W. Grosinger, J. Fellinger, G. Winkler, L.W. Perner, S. Droste, S. H. Salman, C. Li, C.M. Heyl, I. Hartl, O.H. Heckl, Flexible all-PM NALM Yb:fiber laser design for frequency comb applications: operation regimes and their noise properties, Opt. Express 28 (2020) 18946–18968, https://doi.org/10.1364/OE.394543.

[27] Y.X. Ma, S.H. Salman, C. Li, C. Mahnke, Y. Hua, S. Droste, J. Fellinger, A.S. Mayer, O.H. Heckl, C.M. Heyl, I. Hartl, Compact, all-PM fiber integrated and alignment-free ultrafast Yb:fiber NALM laser with sub-femtosecond timing jitter, J. Lightwave Technol. 39 (2021) 4431–4438, https://doi.org/10.1109/JLT.2021.3070208.

[28] S.P. Xiong, D.P. Luo, Y. Liu, W.C. Wang, Z.J. Deng, Z.Q. Tang, G.H. Xie, L. Zhou, Z. Zuo, C.L. Gu, W.X. Li, Investigation of stable pulse mode-locking regimes in a NALM figure-9 Er-doped fiber laser, Opt. Express 31 (2023) 514–527, https://doi.org/10.1364/OE.476630.

[29] G.P. Agrawal, Nonlinear Fiber Optics, firth ed.,, Elsevier/Academic, 2013.

[30] Z. Zhang, T. Zhang, Z.G. Lv, T. Zhang, H.H. Cheng, X.H. Hu, R. Pan, Y. Feng, Y. S. Wang, The route to a 200 MHz, all-PM femtosecond Yb-doped fiber laser with a high output coupling ratio, Appl. Opt. 61 (2022) 8475–8483, https://doi.org/10.1364/AO.472038.

[31] I. Kelson, A.A. Hardy, Strongly pumped fiber lasers, IEEE J. Quantum Electron. 34 (1998) 1570–1577, https://doi.org/10.1109/3.709573.

[32] https://www.thorlabschina.cn/newgrouppage9.cfm?objectgroup_id=15981.

[33] J.F. Li, K.L. Duan, Y.S. Wang, W. Zhao, J.H. Zhu, Y.K. Guo, X.D. Lin, Modeling and effects of ion pairs in high-concentration erbium-doped fiber lasers, J. MOD. Optic. 55 (2008) 447–458, https://doi.org/10.1080/09500340701477776.

[34] L. Grüner-Nielsen, T. Geisler, J. Fini, M.F. Yan, P.W. Wisk, B. Mangan, E.M. Monberg, Polarization maintaining dispersion compensating fiber, in: 2014 European Conference on Optical Communication (ECOC) (2014) https://doi.org/10.1109/ECOC.2014.6963856.

[35] N. Huntemann, C. Sanner, B. Lipphardt, C. Tamm, E. Peik, Single-ion atomic clock with 3×10^{-18} systematic uncertainty, Phys. Rev. Lett. 116 (2016) 063001, https://doi.org/10.1103/PhysRevLett.116.063001.

[36] Z.B. Zhu, G.H. Wu, Dual-comb ranging, Engineering 4 (2018) 772–778, https://doi.org/10.1016/j.eng.2018.10.002.

[37] J. Kim, Y.J. Song, Ultralow-noise mode-locked fiber lasers and frequency combs: principles, status, and applications, Adv. Opt. Photonics 8 (2016) 465–540, https://doi.org/10.1364/AOP.8.000465.

[38] M. Edelmann, Y. Hua, K. Şafak, F.X. Kärtner, Intrinsic amplitude-noise suppression in fiber lasers mode-locked with nonlinear amplifying loop mirrors, Optics Lett. 46 (2021) 1752–1755, https://doi.org/10.1364/OL.415718.